International Journal of Nanomedicine Dovepress

Open Access Full Text Article ORIGINAL RESEARCH

Tooth-Binding Graphene Quantum Dots Silver Nanocomposites for Prevention of Dental Caries

Iris Xiaoxue Yin[1], John Yun Niu[1], May Lei Mei[2], Jinyao Tang[3], William Ka Kei Wu[4], Chun Hung Chu[1]

[1]Faculty of Dentistry, the University of Hong Kong, Hong Kong, People's Republic of China; [2]Department of Oral Rehabilitation, Faculty of Dentistry, University of Otago, Dunedin, New Zealand; [3]Department of Chemistry, the University of Hong Kong, Hong Kong, People's Republic of China; [4]Department of Anaesthesia & Intensive Care, The Chinese University of Hong Kong, Hong Kong, People's Republic of China

Correspondence: May Lei Mei, Department of Oral Rehabilitation, Faculty of Dentistry, University of Otago, Department of Oral Rehabilitation, Faculty of Dentistry, University of Otago, PO Box 56, Dunedin, Otago, 9054, New Zealand, Email may.mei@otago.ac.nz; Chun Hung Chu, Faculty of Dentistry, The University of Hong Kong, Restorative Dental Science, Faculty of Dentistry, The University of Hong Kong, 34 hospital Road, Hong Kong, NA, People's Republic of China, Email chchu@hku.hk

Objective: The objectives of this study were to develop a tooth-binding graphene quantum dots silver nanocomposites (ALN-GQDs-Ag) and evaluate their antibacterial, mineralising, and discolouring properties for the prevention of dental caries.

Methods: In this study, ALN-GQDs-Ag were developed by synthesising nano silver (Ag) with graphene quantum dots (GQDs) and functionalised GQDs with alendronate (ALN). ALN-GQDs-Ag were characterised by transmission electron microscopy (TEM), zeta potential analysis, X-ray photoelectron spectroscopy (XPS), Fourier transform infrared spectroscopy (FTIR), and Raman spectroscopy. The cytotoxicity of ALN-GQDs-Ag against human gingival fibroblasts (HGF-1) and stem cells from human exfoliated deciduous teeth (SHED) was examined using a colorimetric assay with reference to silver nitrate solution. The affinity of ALN-GQDs-Ag for hydroxyapatite particles was investigated using inductively coupled plasma spectroscopy (ICP). The antibacterial properties of ALN-GQDs-Ag against *Streptococcus mutans* were evaluated by scanning electron microscopy (SEM), confocal laser scanning microscopy (CLSM), and colony-forming units counting (CFUs). The mineralisation properties of ALN-GQDs-Ag on human dentine were assessed using micro-computed tomography (micro-CT), scanning electron microscopy (SEM), and Fourier transform infrared in a biochemical cycling model. The discolouring properties of ALN-GQDs-Ag on artificial dentine caries were determined using spectrophotometry.

Results: TEM, Zeta potential, XPS, FTIR, and Raman spectroscopy confirmed the synthesis of stable spherical ALN-GQD-Ag nanocomposites with a 10.3 ± 5.5 nm diameter. The colorimetric assay demonstrated that ALN-GQDs-Ag were less cytotoxic than silver nitrate to HGF-1 and SHED ($p<0.001$). ICP showed that ALN-GQDs-Ag were bound to hydroxyapatite. SEM, CLSM, and CFUs showed that ALN-GQDs-Ag was bactericidal and inhibited biofilm growth of *Streptococcus mutans*. Micro-CT, SEM, and FTIR showed that ALN-GQDs-Ag repressed dentine demineralisation under a cariogenic challenge. Spectrophotometry revealed no significant discolouration of dentine caries in the ALN-GQDs-Ag.

Conclusion: This study developed a biocompatible and tooth-binding ALN-GQDs-Ag with promising antibacterial, mineralising, and non-discolouring properties. ALN-GQDs-Ag could be a novel anti-caries agent for preventing dentine caries if translated for clinical use.

Keywords: graphene quantum dots, silver nanoparticles, caries prevention, antibacterial, mineralisation

Introduction

Dental caries (tooth decay) is one of the most prevalent diseases worldwide.[1] Untreated dental caries can advance into the dental pulp, resulting in dental abscesses, causing discomfort and the spread of infection. Dental caries also has a considerable impact on individuals' nutrition, leading to consequential effects on their growth, development, and overall health.[2] Prevention of dental caries is a continuous and lifelong task, as it can affect individuals of all age groups. Specifically, longer life expectancy prolongs tooth function in the mouth. Dental caries results from an ecological

Received: 12 July 2024
Accepted: 16 October 2024
Published: 3 November 2024

imbalance in the equilibrium between oral microbial biofilms and tooth minerals.[3] The excessive presence of acid-producing bacteria in the mouth is one of the key factors contributing to the development of tooth decay. Colonised cariogenic microbes on tooth surfaces metabolise fermentable carbohydrates, generate organic acids, and create acidic environments. An acidic environment can continuously dissolve hard dental tissue, leading to dental caries. To arrest dental caries, researchers have developed various anti-caries agents to suppress the activity of cariogenic or acid-producing bacteria and to remineralise carious lesions.[4,5]

Antibiotics are frequently used to inhibit bacterial growth and to prevent the spread of dental infection.[6] However, the overuse of antibiotics may lead to the development of bacterial resistance. However, these antibiotics cannot arrest existing caries because of their lack of remineralising properties. Fluoride is widely used for managing dental caries because it effectively promotes the deposition of calcium and phosphate as well as the formation of hydroxyapatite.[7] Owing to its limited antibacterial properties, the effect of fluoride on caries arrest is not ideal. Silver-based solutions such as silver diamine fluoride are alternative methods for managing dental caries.[8] However, the potential for permanent tooth discolouration restricts the use of silver-based solutions.

Nanotechnology is currently under investigation for its numerous practical applications in healthcare and daily life.[9] Silver nanoparticles are a form of nanoparticle that is highly regarded for their wide range of applications, minimal toxicity, absence of bacterial resistance, and exceptional optoelectronic characteristics.[10] Alendronate (ALN) has a prototype biomineral-binding group. Hence, it has a strong affinity for hydroxyapatite which is the primary component of the teeth.[11] This strong interaction was caused by ligand exchange between the two phosphate groups of alendronate and hydroxyapatite. Therefore, alendronate can serve as a stabilising agent for tooth attachment.

Graphene is utilised in many biotechnologies because of its large surface area, simple chemical functionalisation, favourable biocompatibility, and biostability. Graphene has abundant reactive oxygenic groups, such as carbonyl and carboxyl groups on the edges and hydroxyl and epoxide groups on the planes. These reactive oxygenic groups can strengthen the interactions between components at the graphene interface. Additionally, graphene hinders the proliferation of gram-negative (*Pseudomonas aeruginosa*) and gram-positive (*Streptococcus mutans*) bacteria. It also stimulates the formation of hydroxyapatite nanoparticles during bio-mineralisation.[12] Graphene quantum dots (GQDs) belong to the graphene family and are the unique form of zero-dimensional carbon nanomaterials. GQDs are usually smaller than 20 nm in particle size, and can produce a quantum size effect.[13] Among the graphene-based materials, GQDs have more functional groups (eg carboxyl, hydroxyl, carbonyl, and epoxy) for peroxidase-like activity. A series of applications of GQDs have been developed based on their unique physical and chemical properties, such as non-toxicity, solubility, surface grafting, and biocompatibility. GQDs can bind to metal nanoparticles and act as nanocarriers owing to their electronic interactions.[14] In addition, GQDs can be easily functionalised because of abundant oxygen-containing groups in GQDs. These groups can be chemically grafted with various chemicals by conjugated bonding. Thus, GQDs can promote the formation of strong connections between silver nanoparticles and alendronate at the interface.

This study aimed to develop a tooth-binding and non-discoloured graphene quantum dot silver nanocomposites (ALN-GQDs-Ag) and evaluate their antibacterial and mineralising properties for caries prevention. We developed novel graphene quantum dot–silver nanocomposites (ALN-GQDs-Ag) by the in-situ synthesis of silver nanoparticles with graphene quantum dots (GQDs-Ag) and the functionalisation of GQDs-Ag with alendronate (Scheme 1). This ALN-GQDs-Ag was anticipated to have an affinity and non-discolouring effect on teeth and exhibit favourable antibacterial and mineralisation properties.

Materials and Methods

Synthesis of ALN-GQDs-Ag

GQDs were prepared by the pyrolysis of citric acid.[15] Citric acid (Sigma-Aldrich, St Louis, MO, USA) was heated to 200 °C and it melted into an orange-coloured liquid, indicating formation of GQDs. The acidic GQDs liquid was neutralised to pH 7.0 using sodium hydroxide solution (Sigma-Aldrich, St Louis, MO, USA) to form a GQDs suspension (0.4 mg mL^{-1}) under vigorous stirring. Silver nitrate (Sigma-Aldrich, St Louis, MO, USA) was added to

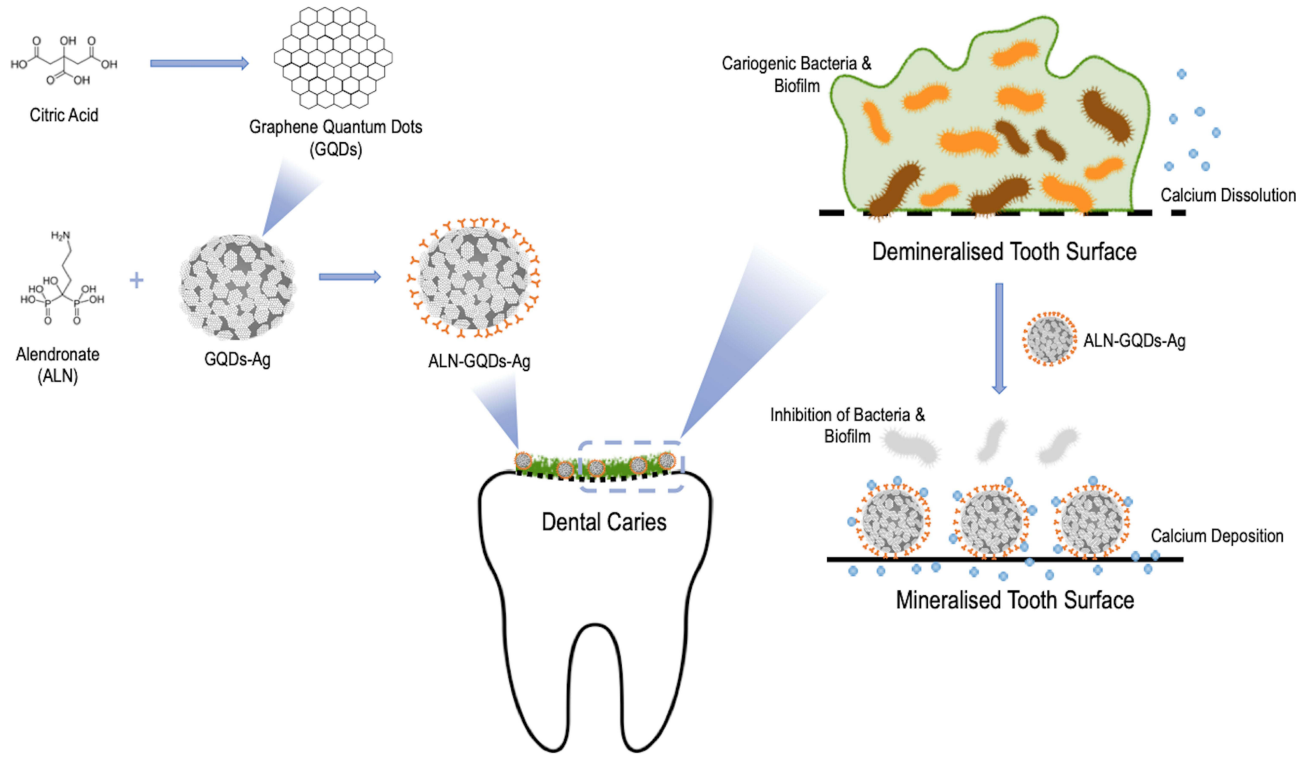

Scheme 1 Schematic illustration of development of tooth-binding graphene quantum dots silver nanocomposites (ALN-GQDs-Ag) for caries prevention. This tooth-binding ALN-GQDs-Ag has promising antibacterial, mineralising and non-discolouring properties. ALN-GQDs-Ag can be a novel anti-caries agent to prevent dentine caries if translated to clinical use.

the suspension and heated at 60 °C to form GQDs-Ag nanocomposites in-situ. The suspension was then washed three times with deionised water to obtain the as-prepared GQDs-Ag.

The GQDs-Ag was incubated with 0.13 mmol 1-Ethyl-3-diaminopropyl carbodiimide (EDC) (Sigma-Aldrich, St Louis, MO, USA) and 0.11 mmol N-hydroxysuccinimide (NHS) (Sigma-Aldrich, St Louis, MO, USA) in 50 mmol phosphate-buffered saline at pH 9 (Sigma-Aldrich, St Louis, MO, USA) at 25 °C under gentle stirring to activate the carboxylic groups. After stirring for 2 h, 0.1 mmol alendronate sodium solution (Sigma-Aldrich, St Louis, MO, USA) was added and the mixture was further stirred for 24 h. The resulting conjugates of ALN-GQDs-Ag were precipitated from the solution to remove unreacted alendronate sodium, NHS, and EDC using a mixture of 50% ethanol, followed by centrifugation at 15,000 rpm for 10 min.

Characterisation of ALN-GQDs-Ag

The size and morphology of the synthesised ALN-GQDs-Ag were characterised by transmission electron microscopy (TEM) (Tecnai G2 20S-TWINScanning, FEI, OR, USA). The surface zeta potential was characterised using Laser Doppler Microelectrophoresis (Zetasizer Nano ZS90, Malvern Panalytical, Malvern, UK). Elemental analysis was performed using energy-dispersive spectroscopy (EDS) with a field emission scanning electron microscope (PHILIPS XL30 CP, Philips, Amsterdam, Netherlands). The elemental composition was analysed by X-ray photoelectron spectroscopy (XPS) (Escalab QXi, Thermo Scientific, MA, USA). The functional groups of ALN-GQDs-Ag were characterised using Fourier transform infrared spectroscopy (FTIR) (Spectrum Two, PerkinElmer, WA, USA). The vibrational modes of carbon in ALN-GQDs-Ag were detected using Raman spectroscopy (Micro-Raman INVIA, Renishaw, UK).

Cytotoxicity of ALN-GQDs-Ag

The cytotoxicity of ALN-GQDs-Ag was evaluated in human gingival fibroblasts (HGF-1) (ATCC) and stem cells from exfoliated deciduous teeth (SHED) (iXCells Biotechnologies).[16] The HGF-1 cells or SHED (1×10^5 mL^{-1}) were cultured

in Dulbecco's modified Eagle's medium containing 10% fetal bovine serum and 1% penicillin for 24 h at 37 °C in 100% humidity and 5% carbon dioxide. The cells were then treated with various concentrations of ALN-GQDs-Ag and silver nitrate. Untreated cells were used as negative controls. After 24 h, the cells were washed with phosphate-buffered saline. The Cell Counting Kit-8 (CCK-8, Apexbio, MA, USA) was used to evaluate cell biocompatibility. The optical density was measured at a wavelength of 450 nm according to protocol provided by manufacturer of kit. The half-maximal inhibitory concentration (IC_{50}), representing the concentration of the experimental solution required for 50% inhibition of the cell viability of ALN-GQDs-Ag and silver nitrate, was measured.

Affinity of ALN-GQDs-Ag

ALN-GQDs-Ag were mixed with hydroxyapatite powder in an artificial saliva solution in Eppendorf centrifuge tubes. The tubes were placed on a Labquake rotator at room temperature to allow binding. At each predetermined time point, the tubes were removed, centrifuged, and 100 μL of the supernatant was collected. The collected samples were diluted 100 times and analysed using inductively coupled plasma–optical emission spectrometry (ICP-OES) (SPECTRO ARCOS, SPECTRO, PA, USA). The amount of silver nanoparticles bound to hydroxyapatite particles was calculated by subtracting the amount of silver remaining in the supernatant from the initial amount of added silver.

Antibacterial Properties of ALN-GQDs-Ag

This study was approved by the Institutional Review Board of the University of Hong Kong/Hospital Authority Hong Kong West Cluster (HKU/HA HKW IRB) (IRB UW21-307), in accordance with the Declaration of Helsinki. Sound human third molars that required removal were collected after obtaining patient consent. Forty dentine slices with a thickness of 2 mm without flaws or other defects were polished and cut into four blocks. Thus, 160 dentine blocks were prepared in total. The blocks were sterilised by autoclaving at 121 °C and then placed in bacterial medium for 3 days to generate artificial caries. The blocks were divided into three groups and received three different topical applications: ALN-GQDs-Ag (containing 4000 ppm Ag) (Group ALN-GQDs-Ag), silver nitrate (containing 4000 ppm Ag) (Group $AgNO_3$), and deionised water (Group Water). All solutions were applied to the block surface using a micro-brush (Micro applicator-regular, Premium Plus International Ltd., Hong Kong, China) for 1 min. The treated blocks were then immersed in 1 mL of bacterial medium consisting of *Streptococcus mutans* bacterial culture in brain heart infusion broth (BHI) and 5% glucose (6×10^8/mL). The blocks were then incubated anaerobically at 37 °C for 6, 12, or 24 h for assessment.

Architecture of the Cariogenic Biofilm

Biofilm morphology was assessed using scanning electron microscopy (SEM) (PHILIPS XL30 CP, Philips, Amsterdam, Netherlands). Three dentine blocks were fixed in 2.5% glutaraldehyde for 4 h at 4 °C, followed by 1% phosphate-buffered saline. After dehydration in a series of ethanol solutions, the blocks were dried in a desiccator and sputter-coated with gold before SEM examination.

Viability of the Cariogenic Biofilm

The viability of the bacteria in the biofilm was assessed using confocal laser scanning microscopy (CLSM) (Fluoview FV 1000, Olympus, Tokyo, Japan). Bacteria on the surfaces of the six dentine blocks were labelled in situ with two fluorescent probes, propidium iodide and SYTO-9 dye (LIVE/DEAD BacLight Bacterial viability kit, Molecular Probes, Eugene, OR, USA). CLSM was used to obtain images of labelled biofilms. The red-to-green ratio was calculated to denote the ratio of dead to live bacteria. A high ratio indicated a positive antimicrobial effect of the studied agent.

Growth Kinetics of the Cariogenic Biofilm

The growth kinetics of biofilms were assessed by counting colony-forming units (CFUs). *Streptococcus mutans* on the surface of six dentine blocks was resuspended in 1 mL of BHI broth. After serial tenfold dilution of the bacterial suspension, each dilution was plated on blood agar. The agars were incubated anaerobically at 37 °C for 48 h before CFUs counting.

Lactic Acid Production

The amount of lactic acid produced by *Streptococcus mutans* biofilms was measured to estimate biofilm cariogenicity. Six dentine blocks were washed twice with phosphate-buffered saline after a 24-hour biofilm challenge. The blocks were immersed in 1.5 mL buffered peptone water supplemented with 0.2% sucrose and incubated at 37 °C in 5% carbon dioxide for 3 h. supernatant was collected from each well and centrifuged for 15 min at 4 °C to remove insoluble material. The lactate concentration in the supernatant was quantified using the lactate dehydrogenase enzymatic method and a lactate dehydrogenase activity assay kit.

Mineralising Properties of ALN-GQDs-Ag

A 7-day biochemical cycling procedure was used for the cariogenic challenge of dentine. Each cycle consisted of a 12-hour biofilm challenge using *Streptococcus mutans* followed by a 12-hour remineralisation using artificial saliva solution (pH 7). The formula for the artificial saliva was 20 mmol 4-(2-hydroxyethyl)-1-piperazineethanesulfonic acid, 1.5 mmol calcium chloride, 0.9 mmol potassium dihydrogen phosphate, and 150 mm potassium chloride. The bacterial medium used was BHI broth with 5% sucrose, and the concentration of the bacterial culture was 6×10^8 cells/mL. Half of the dentine block surface was coated with a nail varnish as an internal control. The dentine blocks were incubated anaerobically at 37 °C in individual cells with 1 mL bacterial medium for three days to generate artificial caries. Before refreshing the demineralising and remineralising solutions, the blocks were washed ultrasonically using sterile deionised water to avoid interference of remaining agents on block surface to experiment results. This step also mimics the effect of the toothbrushing to remove bacteria attached to the block surface in real life. Dentine blocks receive treatment with ALN-GQDs-Ag (containing 4000 ppm Ag) (Group ALN-GQDs-Ag) or deionised water (Group Water as negative control) before each cycle. Each treatment was applied topically for 1 min using a micro-brush. After the cariogenic challenge, dentine blocks were collected for subsequent assessments.

Lesion Depth and Mineral Loss

The lesion depth and mineral loss in the dentine blocks were measured using micro-computed tomography (micro-CT). Two standard phantoms (Bruker, Kontich, Belgium) with mineral density values (MDVs, g cm^{-3}) of 0.25 g cm^{-3} and 0.75 g cm^{-3} were used to calibrate the greyscale. Three-dimensional images of the dentine block were reconstructed and viewed using CTAn software (SkyScan, Antwerp, Belgium). The grayscale values of the demineralised and internal control areas of the six dentine blocks were calibrated and converted into MDVs using CTAn. Mineral loss = MDV of the control region - MDV of the demineralised region.

Surface Morphology

The surface morphology of the dentine blocks was examined using an SEM (Hitachi S-4800 FEG Scanning Electron Microscope; Hitachi Ltd., Tokyo, Japan). Three dentine blocks were washed ultrasonically before assessment to remove the biofilm, dried in a desiccator, and sputter-coated with gold for SEM evaluation.

Chemical Structure

The chemical structures of the dentine blocks were assessed by FTIR spectroscopy. Infrared radiation wavelengths ranging from 500 to 2000 cm^{-1} were used to detect the absorbance of phosphate HPO_4^{2-} (wavelengths between 900 and 1200 cm^{-1}) and amide I (wavelengths between 1585 and 1720 cm^{-1}). The ratio of the areas of the phosphate peak to the amide I peak (HPO_4^{2-}: amide I) for the six dentine blocks was calculated to indicate the extent of dentine demineralisation.

Crystal Characteristics

Diffraction patterns of the dentine blocks were assessed using X-ray diffraction spectroscopy (Bruker AXS GmbH, Karlsruhe, Germany). The International Centre for Diffraction Data (ICDD, PDF-2 Release 2004) was used to check the phase purity and index the chemical phases of the three dentine blocks.

Discolouring Property of ALN-GQDs-Ag

The colour of the dentine blocks was examined using a VITA Easyshade Advance Portable Dental Spectrophotometry (VITA Zahnfabrik GmbH, Bad Säckingen, Germany). The colour of each block was determined according to the

Commission International del'Eclairage L* a* b* colour system. The L* axis represents lightness, ranging from black (0) to white (100); the a* axis represents red (+a*) to green (-a*); and the b* axis represents yellow (+b*) to blue (-b*). Colour assessment of the six dentine blocks was performed before (T0) and after seven 7-day biochemical cycles (T1). The total colour change (ΔE) was calculated using the equation $\Delta E = [(L^*)^2 + (a^*)^2 + (b^*)^2]^{1/2}$.

Statistical Analysis

Normal distribution was assessed for all data using the Shapiro–Wilk test ($p>0.05$). A parametric *t*-test was used to compare the IC_{50}, lesion depth, mineral loss, ratio of phosphate to amide I, and colour change between ALN-GQDs-Ag and silver nitrate. One-way ANOVA with Bonferroni multiple comparison tests was used to compare the red-to-green ratio, log CFUs, and lactic acid production among the different groups. IBM SPSS V20.0 software (IBM Corporation, Armonk, NY, USA) was used to analyse all the data, and the level of significance was set at 5%.

Results

Characterisation of ALN-GQDs-Ag

The TEM images in Figure 1a and b show the formation of spherical monodisperse ALN-GQDs-Ag. The mean size of ALN-GQDs-Ag was 10.32 ± 5.45 nm. The zeta potential of ALN-GQDs-Ag was −53.2 mV in Figure 1c. The high

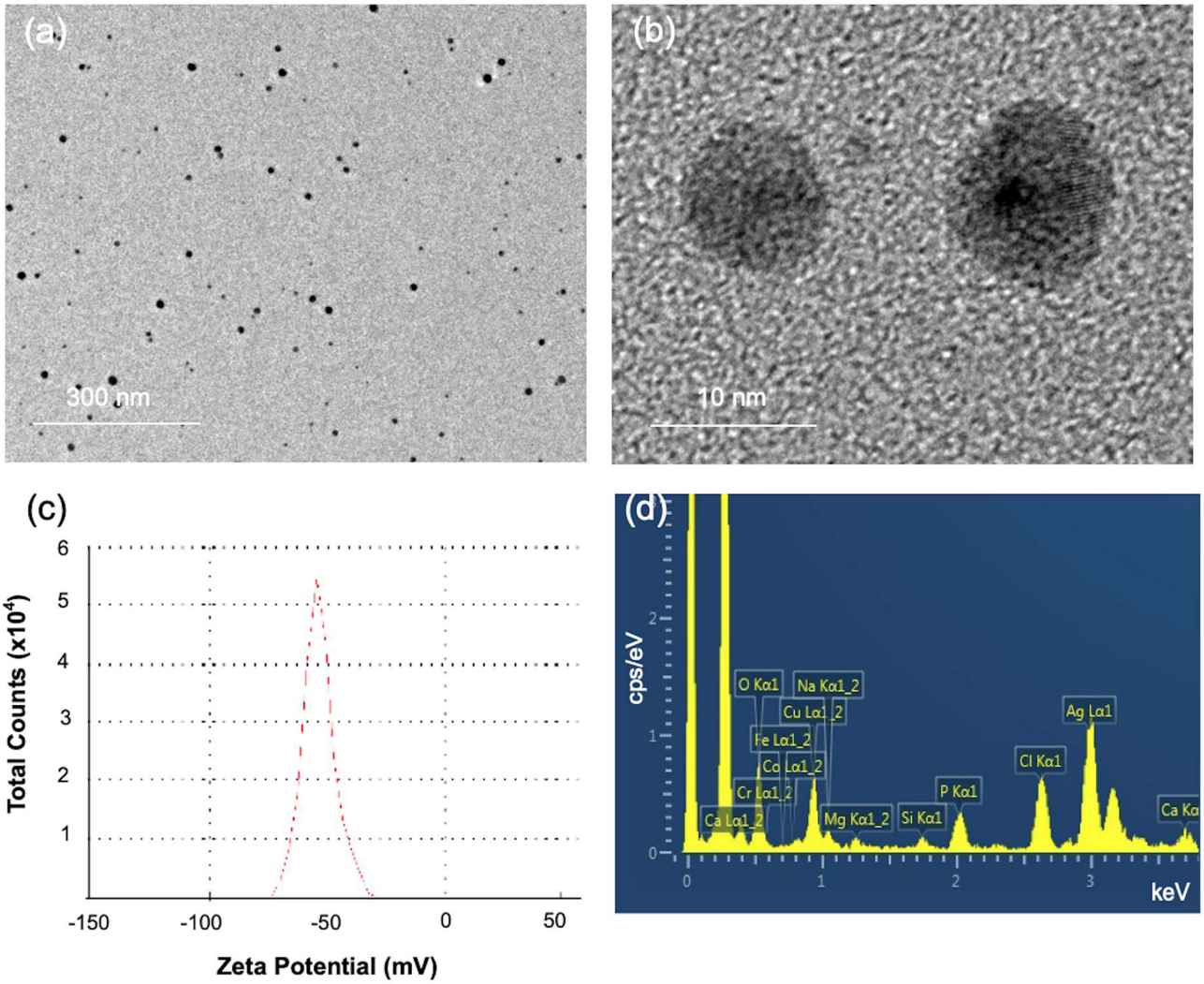

Figure 1 TEM images (**a** and **b**), zeta potential distribution (**c**), and EDS spectrum (**d**) of ALN-GQDs-Ag. TEM showed homogenous spherical ALN-GQDs-Ag particles (**a**) with 10 nm diameter (**b**). Zeta potential (**c**) showed the particles had a surface charge of 53 mV. EDS spectrum (**d**) showed presence of silver (Ag), phosphorus (P) and nitrogen (N) in the particles.

surface zeta potentials suggest high dispersion stability of the synthesised ALN-GQDs-Ag. The EDS spectrum shows the Ag and P elements of ALN-GQDs-Ag in Figure 1d which implies that alendronate was conjugated with the GQDs-Ag nanoparticles.

The XPS spectra showed a full survey scan of the GQDs, GQDs-Ag, and ALN-GQDs-Ag, as shown in Figure 2a. The major peaks of the GQDs at 284.8 and 531.0 eV correspond to C1s and O1s. The obvious peaks at 367.8 eV in the spectrum of the GQDs-Ag indicate the presence of Ag3d. The spectrum of ALN-GQDs-Ag shows C1s, Ag3d, N1s, and O1s peaks at 532.3, 399.0, 368.0 and 284.8 eV, respectively. The high-resolution spectrum of C1s in Figure 2b was deconvoluted into four peaks at 284.8, 285.9, 287.2 and 288.8 eV, which can be attributed to chemical bonds –H, C-C, O=C-N, and O=C-O, respectively. The high-resolution spectrum of N1s in Figure 2c comprises three overlapping peaks at 399.8, 401.2 and 402.2 eV respectively, which are attributed to chemical bonds–C, N-H, and N-C=O bonds, respectively. The high-resolution spectrum of Ag3d in Figure 2d revealed two spin-orbit peaks at 367.9 and 373.9 eV, corresponding to 3/2 and 5/2 spin states. The difference between the $Ag3d_{5/2}$ and $Ag3d_{3/2}$ signals was 6 eV, indicating the metallic nature of Ag.

The Raman spectra of the GQDs showed two principal bands at 1372 cm^{-1} and 1613 cm^{-1} (Figure 3), corresponding to the D and G bands. The intensity ratios of the D and G bands (I_D/I_G) of the GQDs, GQDs-Ag, and ALN-GQDs-Ag are 0.90, 0.93, and 0.95, respectively. The intensity of the bands of GQDs-Ag and ALN-GQDs-Ag increased by over 600% in comparison to the GQDs, indicating the surface-enhanced Raman spectroscopy activity of the GQDs.

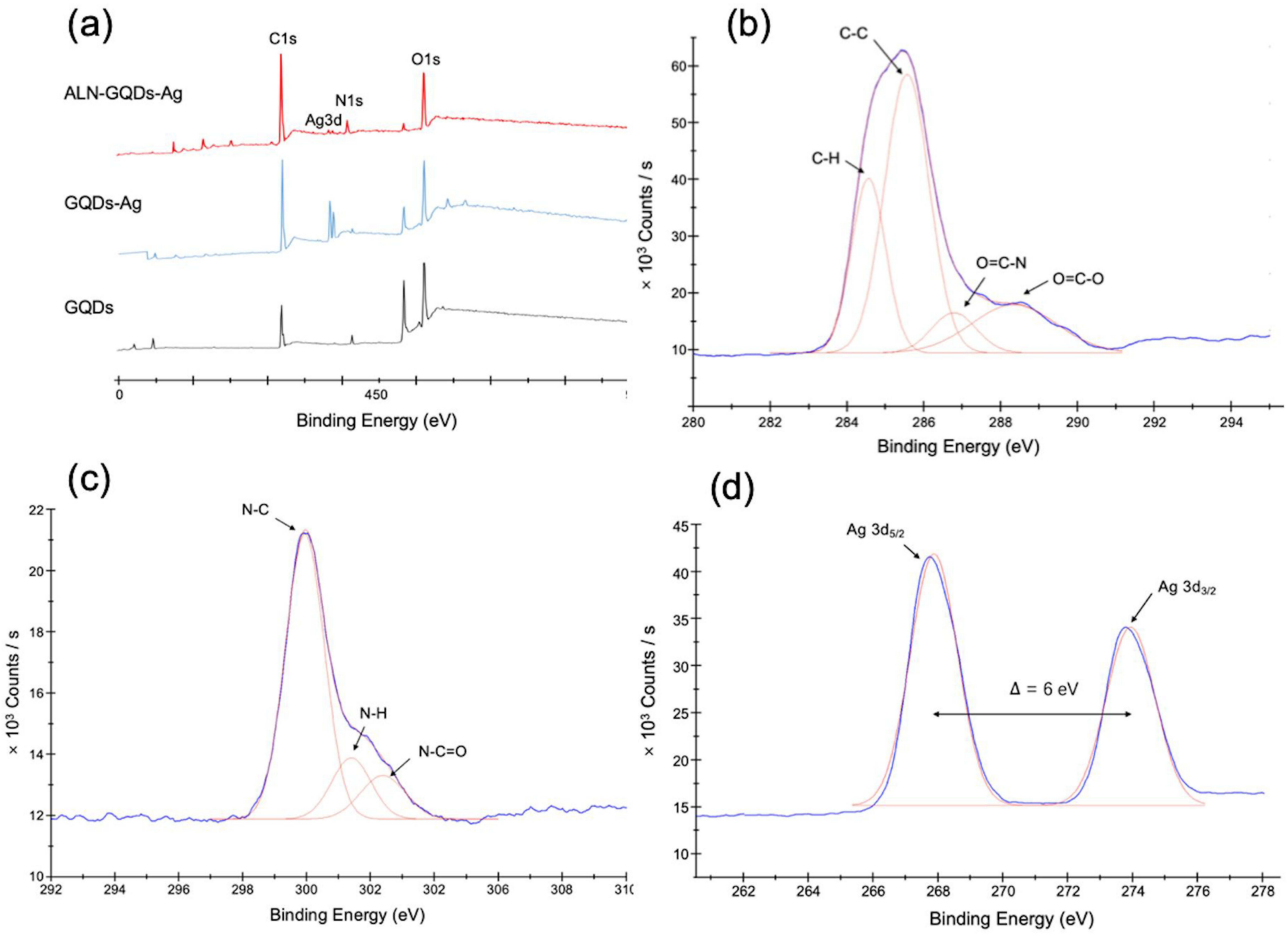

Figure 2 XPS spectra showing full survey scan of GQDs, GQDs-Ag and ALN-GQDs-Ag (**a**), and high-resolution spectra of ALN-GQDs-Ag at C1s (**b**), N1s (**c**) and Ag3d (**d**). XPS spectrum of ALN-GQDs-Ag showed the peaks of C, N, O and Ag representing the presence of these elements in the graphene (**a**). High-resolution spectra showed the chemical bonds of C (**b**) and N (**c**) and the presence of metallic Ag (**d**).

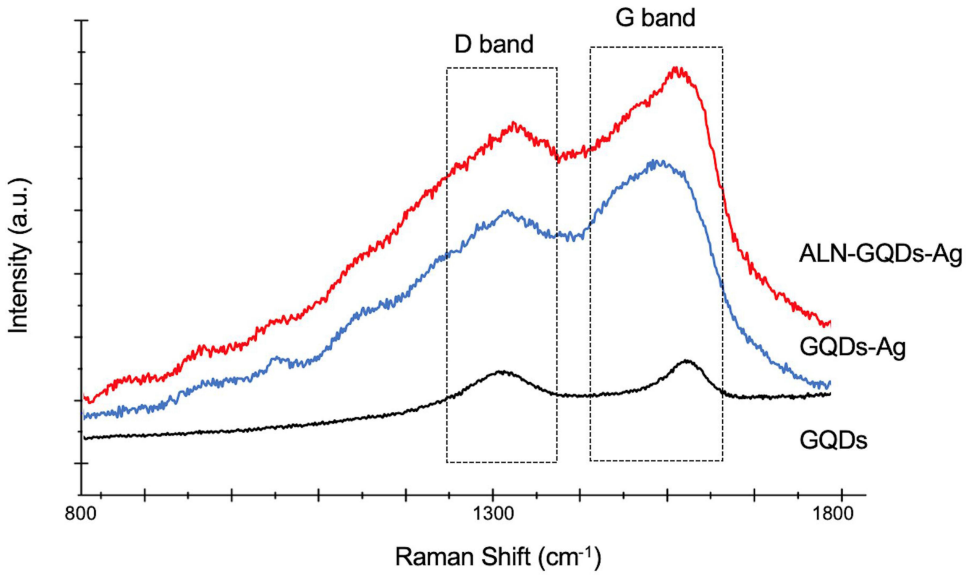

Figure 3 Raman spectra of GQDs, GQDs-Ag and ALN-GQDs-Ag. D band (defect-induced peak at 1372 cm-^{1}) and G band (graphitic peak at 1613 cm-^{1}) are characteristic bands for graphene materials.

The FTIR spectra of the GQDs, GQDs-Ag, and ALN-GQDs-Ag showed -OH and -C-O- groups at 3464 and 11 25 cm^{-1}, respectively (Figure 4), indicating the presence of hydroxyl groups. The peaks at 1580 and 1397cm^{-1} corresponding to the -COO- group, indicated the presence of carboxyl groups. In addition to the hydroxyl and carboxyl peaks, the spectrum of ALN-GQDs-Ag also showed primary and secondary carbonamide bands (-N-C=O) at 1653 and 1572 cm^{-1}, further confirming the amide linkages between the GQDs and ALN.

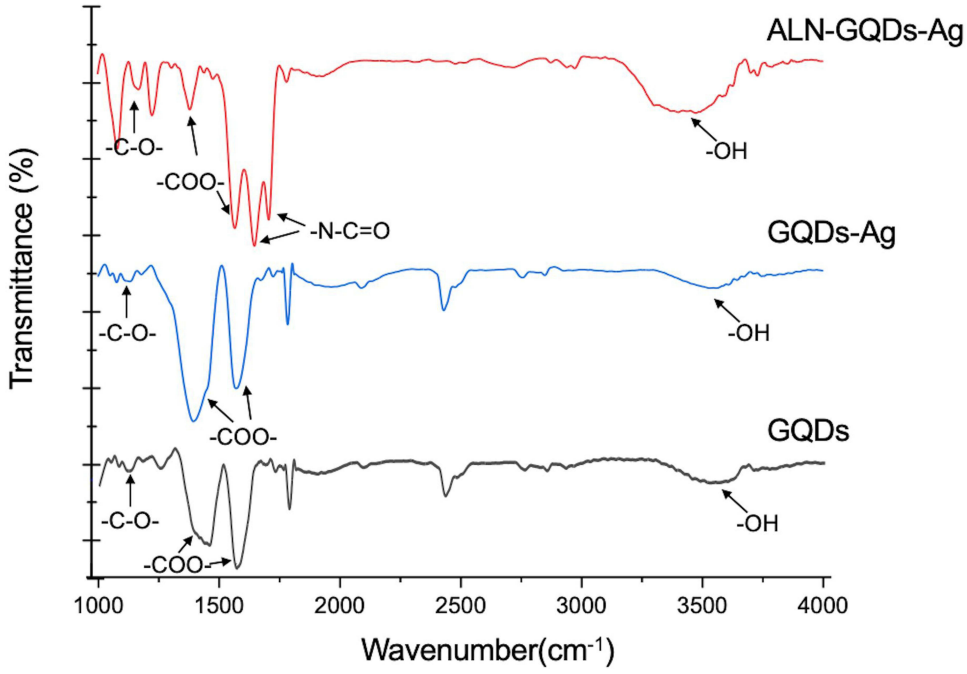

Figure 4 The FTIR spectra of GQDs, GQDs-Ag and ALN-GQDs-Ag. The top (red) spectrum showed the presence of carboxyl (-COO-), carbonamide (-N-C=O) and hydroxyl (-OH) groups of ALN-GQDs-Ag.

Table 1 The IC_{50} Values (Concentration of Silver) of ALN-GQDs-Ag and $AgNO_3$

Group	ALN-GQDs-Ag	$AgNO_3$	*p* value
HGF-1	50.61 ± 15.33	11.42 ± 5.31	< 0.001
SHED	54.30 ± 16.95	14.43 ± 7.23	< 0.001

Cytotoxicity

The IC_{50} values of ALN-GQDs-Ag to HGF and SHED were 50.61 ± 15.33 and 54.30 ± 16.95 ppm. The IC_{50} values of silver nitrate to HGF and SHED were 11.42 ± 5.31 and 14.43 ± 7.23 ppm. The IC_{50} values of ALN-GQDs-Ag for HGF-1 and SHED were significantly higher than those for silver nitrate ($p < 0.001$, Table 1).

Tooth-Binding Property of ALN-GQDs-Ag

The percentages of GQDs-Ag and ALN-GQDs-Ag binding to hydroxyapatite shown in Figure 5. After 10-minute mixture, 75% ALN-GQDs-Ag bound to hydroxyapatite powder and maintained a binding rate of over 90% after 20 min. The maximum binding percentage of ALN-GQDs-Ag is 94% after 60 min. Only 61% of the GQDs-Ag were bound to the hydroxyapatite powders after 10-minute mixture. The maximum binding percentage of GQDs-Ag is 64%.

Antibacterial Effect of ALN-GQDs-Ag

The SEM images showed that dentine treated with ALN-GQDs-Ag did not show noticeable accumulation of *Streptococcus mutans* at any time point (Figure 6). Dentine treated with silver nitrate showed obvious bacterial accumulation at 12 h and biofilm formation at 24 h with extracellular matrix-like structures. Biofilms were formed on the dentine treated with water for 6 h.

CLSM images displayed obvious red fluorescence (dead cells) and scattered green fluorescence (live cells) of *Streptococcus mutans* distributed on dentine treated with ALN-GQDs-Ag (Figure 7). Red fluorescence was rarely

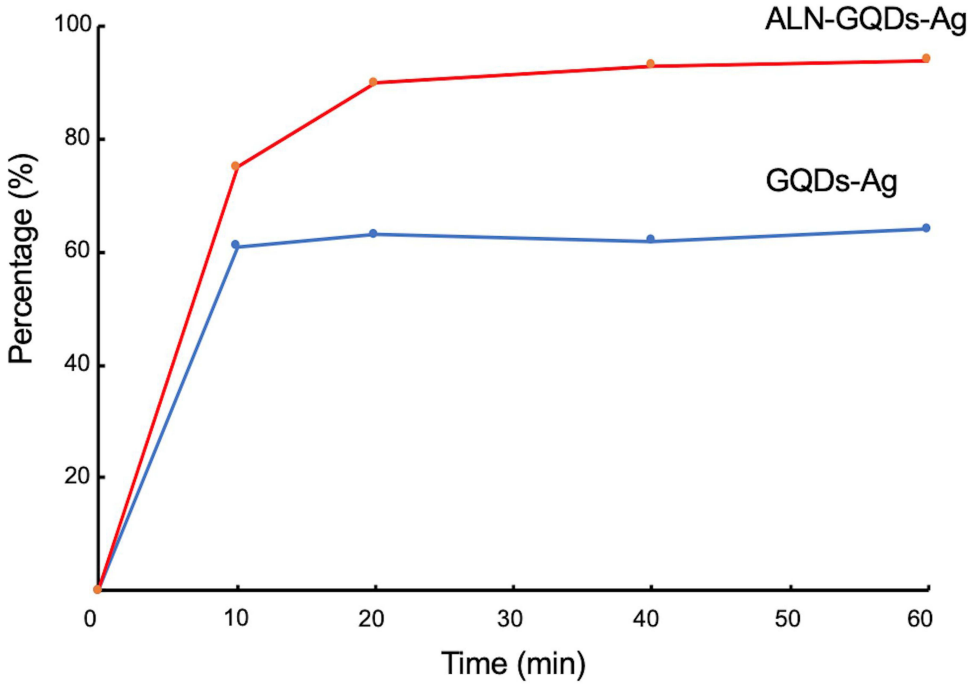

Figure 5 The percentage of ALN-GQDs-Ag and GQDs-Ag binding to hydroxyapatite over 60 minutes. The maximum binding percentages of ALN-GQDs-Ag and GQDs-Ag to hydroxyapatite were 94% and 64%.

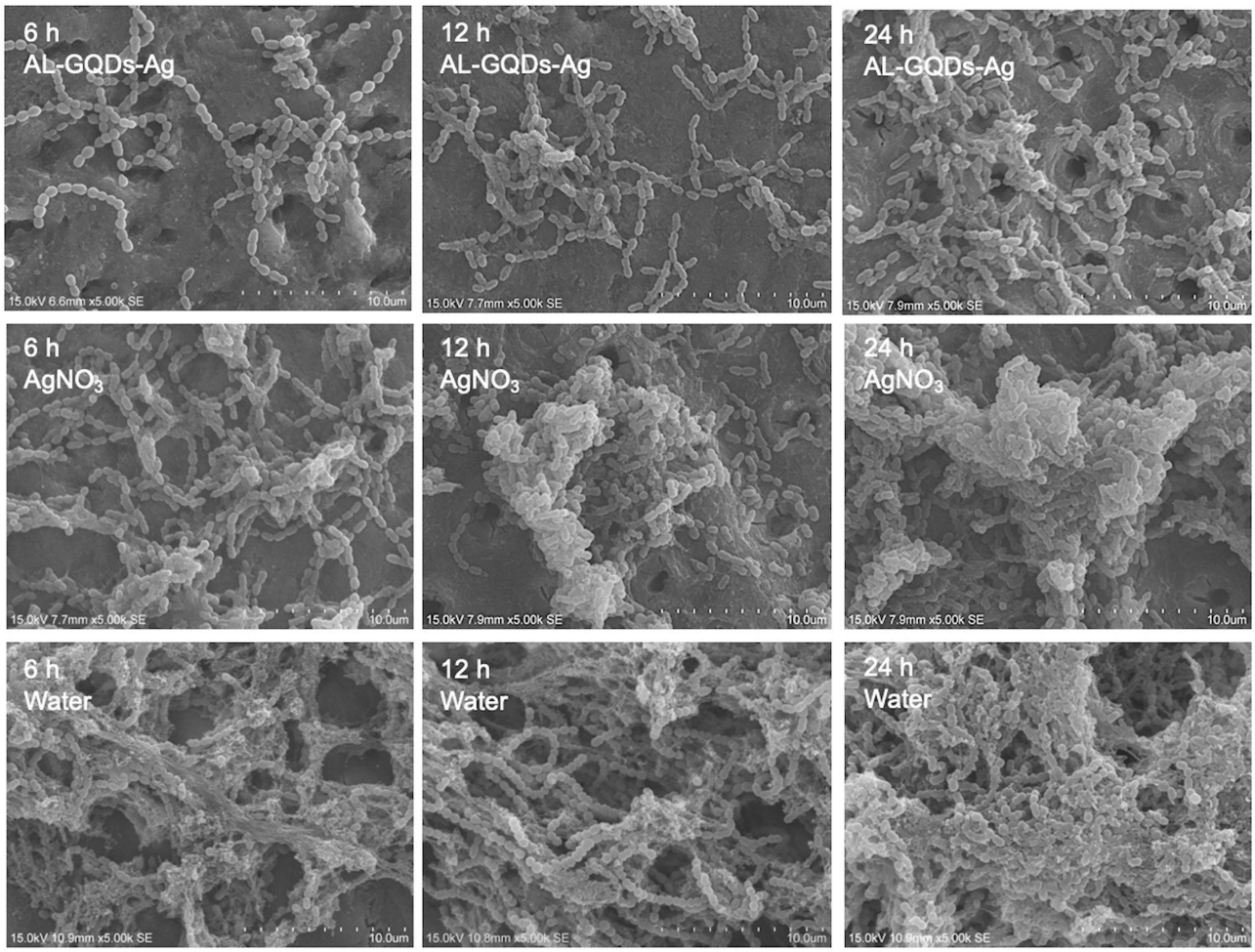

Figure 6 SEM images of S. mutans biofilm on dentine treated with ALN-GQDs-Ag, AgNO3 and water at 6, 12 and 24 hours. The micrographs show scant bacterial colonies scattered across the dentine surface treated with ALN-GQDs-Ag, and confluent growth of biofilm on dentine treated with AgNO3 at 24 hours and dentine treated with water at 6 hours.

observed, and green fluorescence overlapped on dentine treated with silver nitrate for 24 h. Green fluorescence covered the entire surface of the dentine treated with water. The red-to-green ratios in Table 2 reveal the consistent results observed in the CLSM images. The red-to-green ratio of dentine treated with ALN-GQDs-Ag was significantly higher than that of dentine treated with silver nitrate or water at all the time points ($p < 0.001$).

The common logarithm of CFUs was calculated to determine the kinetics of the biofilm (Table 3). The log CFUs on dentine treated with ALN-GQDs-Ag were significantly lower than those treated with silver nitrate or water at all time points ($p < 0.001$, Table 3). The lactic acid produced on dentine treated with ALN-GQDs-Ag, silver nitrate and water were 1.86 ± 0.20, 2.32 ± 0.19 and 2.58± 0.23 ($p < 0.001$, Group ALN-GQDs-Ag < Group $AgNO_3$ < Group Water).

Mineralisation Effects of ALN-GQDs-Ag

Typical micro-CT images and reconstructed three-dimensional images showed the lesion depth and mineral loss of the dentine blocks are shown in Figure 8. Dentine treated with water showed a greater lesion depth than that treated with ALN-GQDs-Ag. In Table 4, the lesion depths of dentine treated with ALN-GQDs-Ag and water were 109.19 ± 25.62 μm and 200.24 ± 26.52 μm, respectively ($p < 0.001$). The mineral loss of dentine treated with ALN-GQDs-Ag and water were 0.62 ± 0.06 g cm^{-3} and 1.02 ± 0.08 g cm^{-3}, respectively ($p < 0.001$).

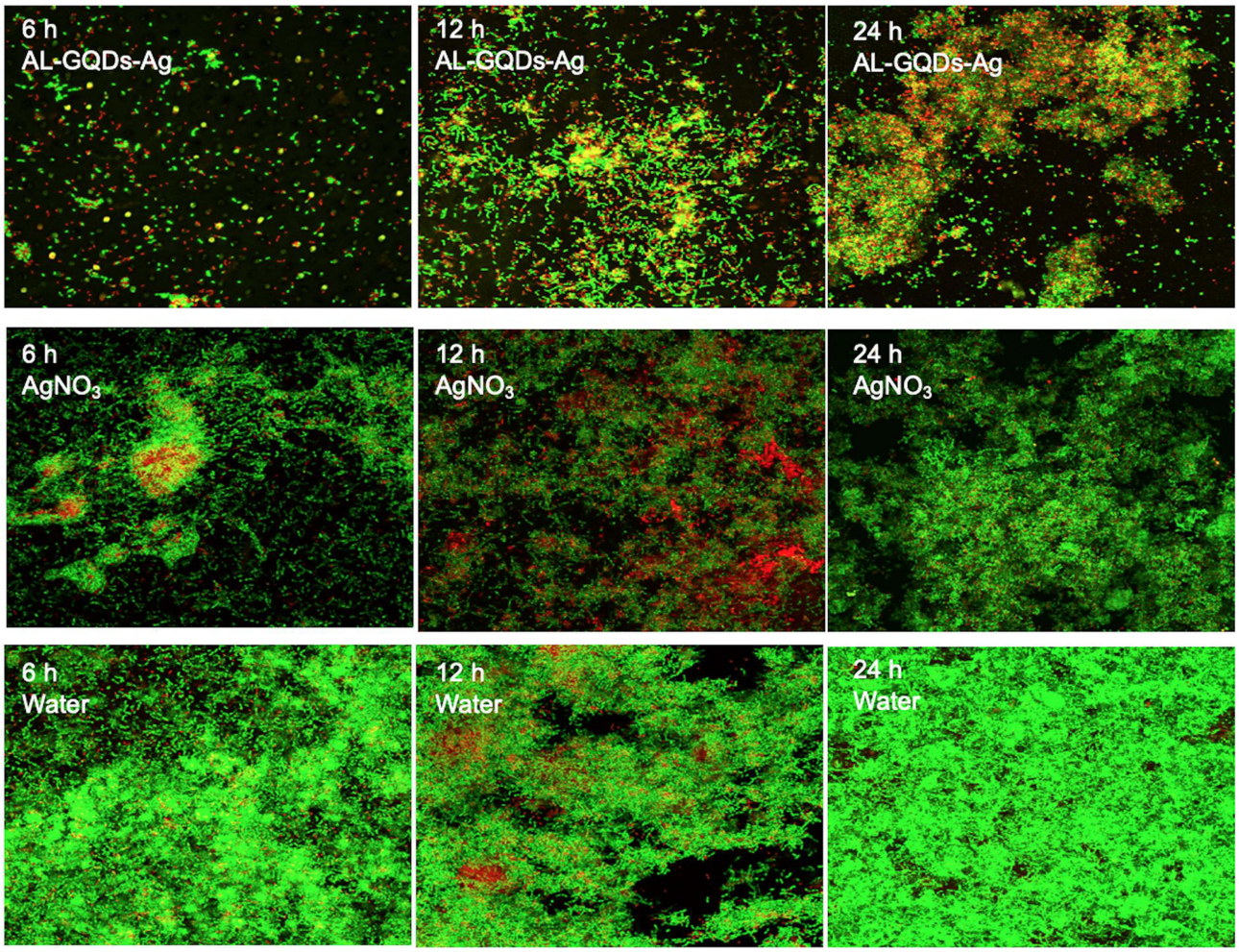

Figure 7 The CLSM images of biofilm on dentine treated with ALN-GQDs-Ag, $AgNO_3$ and water at 6, 12 and 24 hours. The proportion of area of green fluorescence (live cell) was low, whereas the proportion of area of red fluorescence (dead cell) was high on the surface of dentine treated with ALN-GQDs-Ag.

The SEM images in Figure 9 reveal that collagen fibres were severely exposed and fractured on the surface of dentine treated with water, whereas the collagens were slightly exposed and orderly distributed on the surface of dentine treated with ALN-GQDs-Ag.

The FTIR spectra exhibited a strong intensity of the phosphate band on dentine treated with ALN-GQDs-Ag (Figure 10). The ratios of HPO_4^{2-}: amide I absorbance of dentine treated with ALN-GQDs-Ag and water were 0.54 ± 0.08 and 0.38 ± 0.07, respectively ($p = 0.04$). The ratio values indicated that demineralised dentine treated with water had a larger amount of exposed collagen than dentine treated with ALN-GQDs-Ag.

The XRD spectra show diffraction peaks at 25.8°, 31.8°, 32.2°, and 32.8°, corresponding to the peaks for hydroxyapatite (002, 211, 112, and 300) in Figure 11. The low intensities of peaks 211, 112, and 300 on dentine treated with water indicate the loss of crystallinity of dentine. In addition, silver chloride (200 and 220) was identified at 32.2° and

Table 2 The Red-to-Green Ratios of Biofilm on Dentine Treated with ALN-GQDs-Ag, $AgNO_3$ and Water at 6, 12 and 24 hours

Time	ALN-GQDs-Ag[1]	$AgNO_3$ [2]	Water [3]	*p* value	Multiple Comparisons
6 h	1.36 ± 0.28	1.04 ± 0.15	0.84 ± 0.09	<0.001	1>2>3
12 h	0.70 ± 0.13	0.61 ± 0.16	0.39 ± 0.22	<0.001	1>2>3
24 h	0.36 ± 0.14	0.43 ± 0.13	0.23 ± 0.12	<0.001	1>2, 3

Table 3 Log CFUs of Biofilm on Dentine Treated with ALN-GQDs-Ag, $AgNO_3$ and Water at 6, 12 and 24 hours

Time	ALN-GQDs-Ag[1]	$AgNO_3$ [2]	Water [3]	*p* value	Multiple Comparisons
6 h	3.85 ± 0.09	4.19 ± 0.12	4.53 ± 0.28	<0.001	1<2<3
12 h	4.86 ± 0.20	5.42 ± 0.24	6.66 ± 0.19	<0.001	1<2<3
24 h	5.11 ± 0.27	6.58 ± 0.28	7.77 ± 0.38	<0.001	1<2, 3

46.3°, respectively, in dentine treated with ALN-GQD-Ag. The peak at 38.18° indicated the presence of silver (111) on dentine treated with ALN-GQDs-Ag, implying the presence of metallic silver.

Colour Test

Intragroup analysis of b* and lightness (L*) values of dentine treated with ALN-GQDs-Ag ($p = 0.16$) and dentine treated with water ($p = 0.10$) showed no significant difference before and after treatment. Both groups displayed an obvious decrease in the a* value ($p < 0.05$) (Table 5). There was no significant difference ($p = 0.54$) between the ΔE of dentine treated with ALN-GQDs-Ag (ΔE = 6.18 ± 3.45) and dentine treated with water (ΔE = 5.24 ± 2.43).

Discussion

We successfully developed tooth-binding and non-discoloured ALN-GQDs-Ag with antibacterial and mineralising properties for caries prevention. The results of this study demonstrated that ALN-GQDs-Ag has low toxicity towards oral cells and affinity for hydroxyapatite, which is the main component of teeth. ALN-GQDs-Ag has promising antibacterial properties against *Streptococcus mutans* biofilms and mineralising properties without tooth staining.

Strategies for developing GQDs significantly affect their chemical and physical properties. To date, the synthesis methods for GQDs can be classified into two categories: top-down and bottom-up methods. The top-down method refers

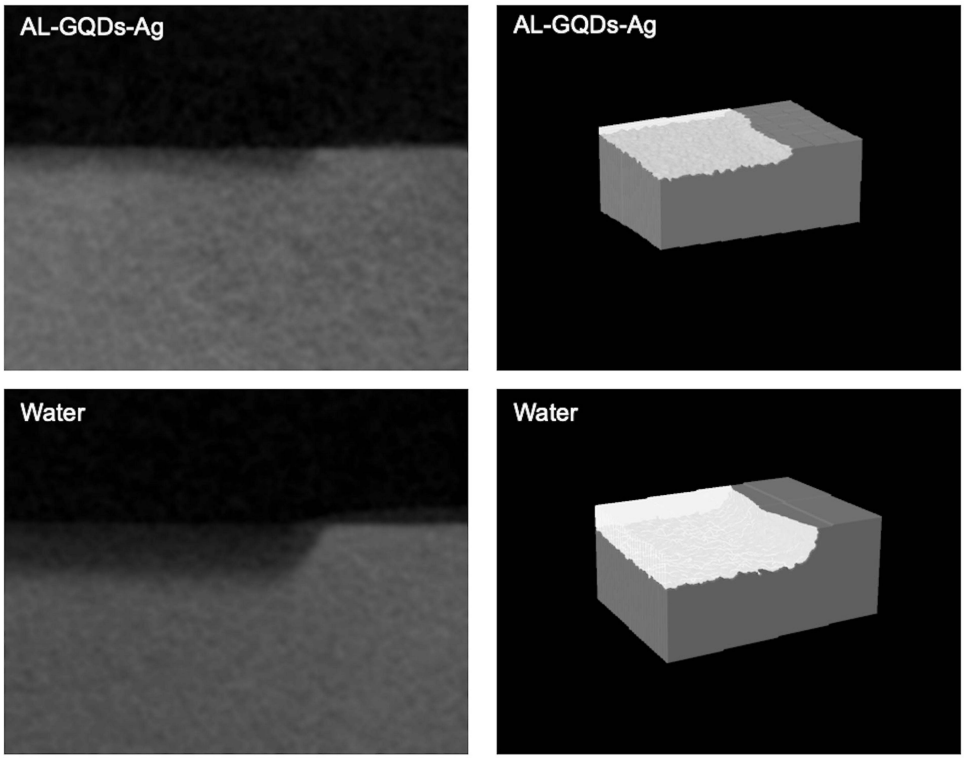

Figure 8 Micro-CT (left) and reconstructed 3-D images (right) of dentine treated with ALN-GQDs-Ag and water. The ALN-GQDs-Ag-treated dentine shows less demineralisation than that treated with water.

Table 4 The Lesion Depths and Mineral Loss of Dentine Treated with ALN-GQDs-Ag and Water

Assessment of dentine	ALN-GQDs-Ag	Water	*p* value
Lesion depth (μm)	109.19 ± 25.62	200.24 ± 26.52	<0.001
Mineral loss (g cm^{-3})	0.62 ± 0.06	1.02 ± 0.08	<0.001

to the direct cutting of graphene-related materials such as graphene, graphene oxide and graphite into quantum sizes.[17] GQDs developed via the top-down method usually suffer from some disadvantages, such as low yield, critical synthesis conditions, and difficulty in controlling the size distribution of the products. Therefore, in this study, we used a bottom-up method to develop GQDs by carbonising citric acid via thermal treatment. This method can precisely control the morphology and size of developed GQDs.[15] The Raman spectra in Figure 3 reveal the presence of the D band (1372 cm^{-1}) and G band (1613 cm^{-1}) which are the characteristic peaks of graphene-based nanomaterials. The D band which arises from doubly bonded carbon atoms (C=O), represents the degree of disorder. The G band which arises from singly bonded carbon atoms (C-OH), represents the level of the structural order. The ratio of the D and G band intensities (I_D/I_G) is a measure of the defects present in the graphene structure and can be used to determine the

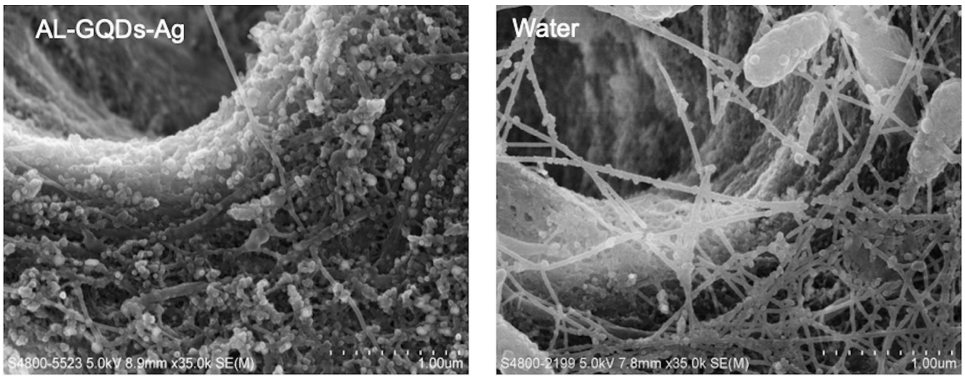

Figure 9 SEM images of dentine treated with ALN-GQDs-Ag and water. The ALN-GQDs-Ag-treated dentine shows less collagen exposure than that treated with water.

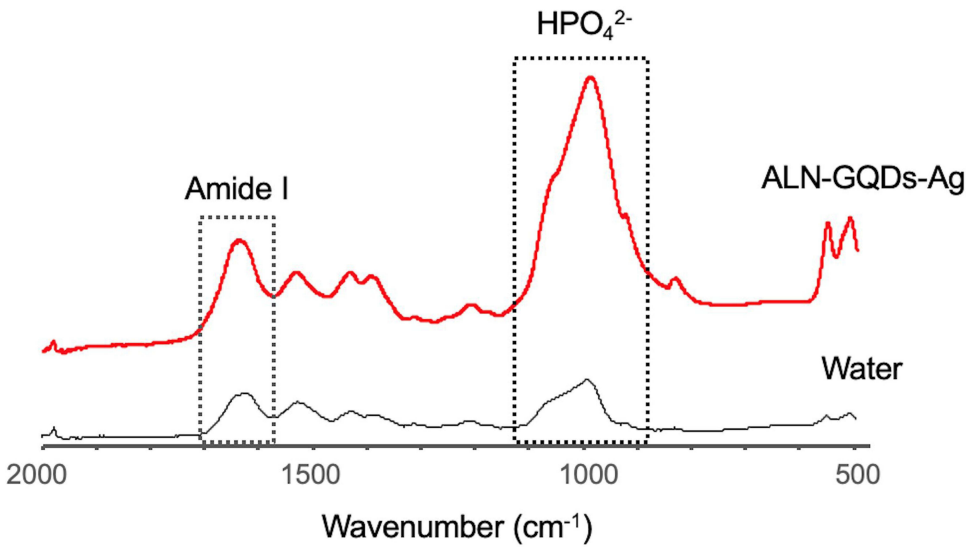

Figure 10 FTIR spectra of the dentine treated with ALN-GQDs-Ag and water. The ALN-GQDs-Ag-treated dentine shows a higher ratio of phosphate to amide I than that treated with water, indicating a higher degree of mineralisation.

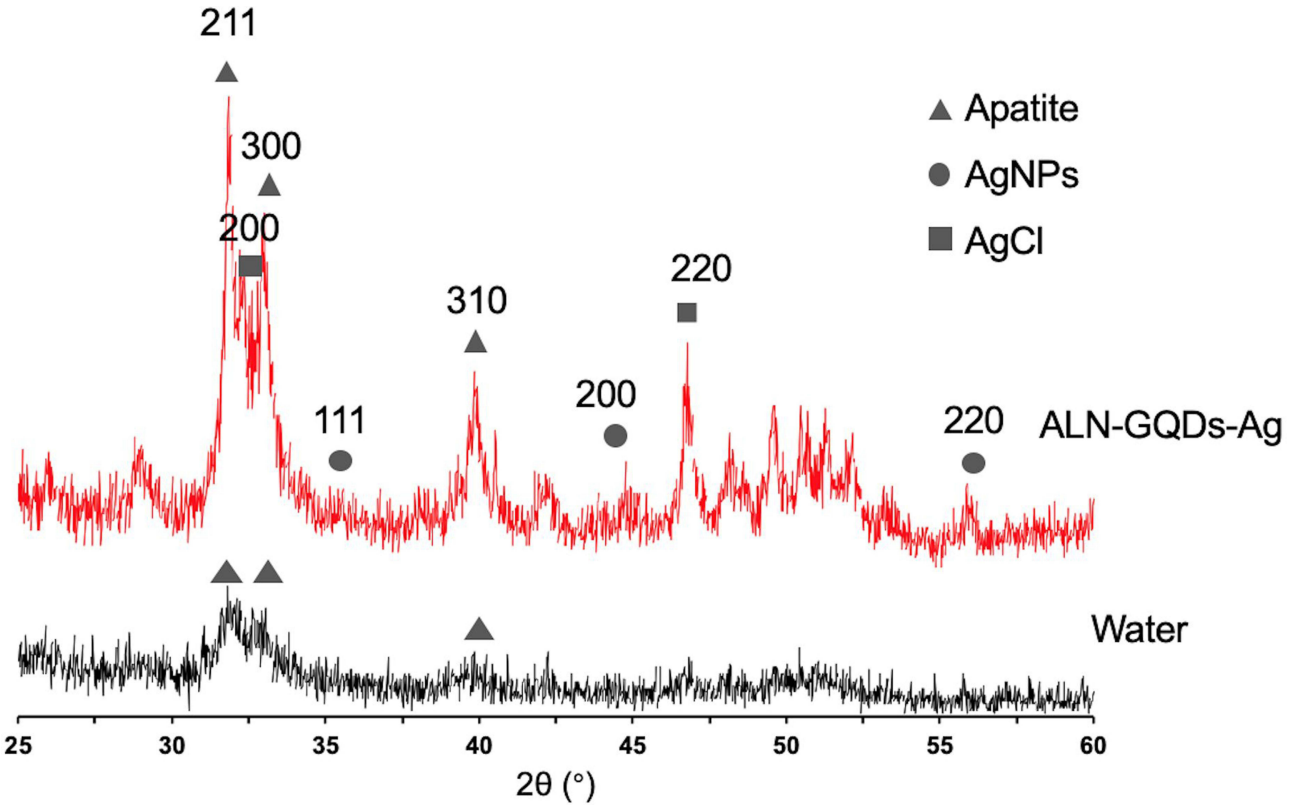

Figure 11 X-ray diffraction patterns of the dentine treated with ALN-GQDs-Ag and water. The peaks of 002, 211, 112 and 300 represented the presence of hydroxyapatite. Dentine treated with ALN-GQDs-Ag had peaks of silver chloride (200 and 220) and metallic silver (111).

quality of the graphene.[18] The intensity ratio of the D and G bands of the developed GQDs was calculated as 0.90 which is ideal.

In this study, we use FTIR to analyse the functional groups of ALN-GQDs-Ag with attenuated total reflection (ATR) technique. The attenuated total reflection (ATR) and diffuse reflectance infrared Fourier transform (DRIFT) are two sample preparation techniques used as alternatives to transmission FTIR. They are less variable, cost and labour-intensive than transmission FTIR. ART provide more reliable results than DRIFT and produce similar spectra with transmission FTIR.[19] The FTIR spectra in Figure 4 also show obvious -OH and -C-O- bands of the GQDs at 3464 and 11 25 cm^{-1}, which indicate the presence of hydroxyl groups. The bands of the-COO- groups detected in the GQDs spectra at 1580 and 1397cm^{-1} also imply the presence of carboxyl groups. These results confirm that the developed GQDs had abundant oxygen functional groups for further functionalisation. The presence of the -COO- group was also detected using high-resolution XPS. In this study, we used GQDs as both a reducing agent and stabiliser for the reduction of silver ions to silver nanoparticles. The formation of silver nanoparticles was observed in high-resolution XPS spectra (Figure 2). The

Table 5 Coordinates (L* a* B*) of Dentine Before Treatment of ALN-GQDs-Ag and Water and After 7-Day Biochemical Cycles

Group	Coordinates	Before	After	*p* value	ΔE
ALN-GQDs-Ag	L*	59.50 ± 2.40	58.22 ± 3.85	0.16	6.18 ± 3.45
	a*	19.66 ± 5.01	15.66 ± 0.91	0.006	
	b*	33.26 ± 2.87	31.97 ± 3.57	0.16	
Water	L*	54.22 ± 4.20	53.59 ± 3.42	0.10	5.24 ± 2.43
	a*	19.93 ± 3.38	17.09 ± 0.79	0.003	
	b*	30.97 ± 1.78	29.46 ± 5.15	0.37	

differences between the Ag3d5/2 and Ag3d3/2 signals indicate the metallic nature of Ag. The ratio of the D and G band intensities of the GQDs-Ag increased to 0.93. This indicates that the sp2 carbon bonds are broken and that there are more sp3 carbon bonds which indicates the reduction of C-O groups in GQDs after the in-situ growth of silver nanoparticles. The band intensity of the GQDs-Ag also increased in comparison to that of the GQDs owing to GQDs doping on the silver nanoparticle surface. Researchers have found that the in situ growth of silver nanoparticles on the surface of GQDs facilitates the favourable dispersion of nanoparticles and improves their stability in aqueous media.[20] After the synthesis of GQDs-Ag, alendronate was conjugated with the GQDs-Ag. The activated carboxylic groups in GQDs react with the amino group in alendronate to form amide linkages.[21] The C1s spectrum of the high-resolution XPS in Figure 2b shows the O=C-N group and the N1s spectrum in Figure 2C shows the N-C, N-H, and N-C=O groups. In addition, the FTIR spectra of the ALN-GQDs-Ag showed primary and secondary carbonamide bands (O=C-N). The XPS and FTIR results confirmed the formation of amide linkages between the GQDs and alendronate and the synthesis of ALN-GQDs-Ag.

Streptococcus mutans is an important cariogenic bacterium involved in the development of dental caries. *Streptococcus mutans* is highly acidogenic. They can produce short-chain carboxylic acids that dissolve the mineral components of dental hard tissue. Moreover, *Streptococcus mutans* can ferment sucrose and produce extracellular polysaccharides which enhances bacterial adherence to tooth surfaces and facilitate biofilm formation. *Streptococcus mutans* biofilms are one of the most common microbial models used in caries research.[16] This study revealed that ALN-GQDs-Ag has a superior antibacterial effect against *Streptococcus mutans* biofilms compared to silver nitrate at the same concentration of silver. Silver nanoparticles exhibit promising antibacterial activity even at low concentrations owing to their large surface-to-volume ratio. Although the exact mechanism underlying the antibacterial effects of silver nanoparticles has not been entirely clarified, various antibacterial actions have been proposed. Silver nanoparticles disrupt the cell wall and cytoplasmic membrane.[22] They can also accumulate in cell wall pits or move directly across the cytoplasmic membrane. Eventually, Silver nanoparticles cause membrane denaturation and the release of organelles from the cell. Silver nanoparticles denature ribosomes and bind deoxyribonucleic acid. Deoxyribonucleic acid replication, protein synthesis, and cell multiplication were inhibited. The dissolution efficiency of silver nanoparticles strongly affects their antibacterial effects. Smaller Silver nanoparticles in spherical or quasi-spherical formats are more prone to silver release because of their larger surface area.[23] This also explains the lower silver release by the aggregated nanoparticles relative to the isolated nanoparticles. Capping agents are used to modify the surfaces of silver nanoparticles, which can change their dissolution behaviour and prevent their aggregation of silver nanoparticles. In this study, we used GQDs as reducing and capping agents to develop spherical and stable silver nanoparticles without aggregation. Owing to the lack of affinity to the tooth surface, silver nanoparticles cannot efficiently adsorb on the surface of the tooth and maintain a long-lasting antibacterial effect. Alendronate is specifically adsorbed on hydroxyapatite.[24] It has been used as a drug carrier to endow other materials with special hydroxyapatite-binding ability to develop bone- or tooth-targeted drug delivery systems. Thus, in this study, alendronate was conjugated with GQDs to increase the binding strength between GQDs-Ag and the surface of dental hard tissue. The tooth-binding test indicated that ALN-GQDs-Ag had a higher binding rate (95%) than that of GQDs-Ag (65%). Alendronate reinforced the binding ability of GQDs-Ag to the tooth surface, prolonging the antibacterial effect of ALN-GQDs-Ag. In this study, ALN-GQDs-Ag had a stronger inhibitory effect than silver nitrate against *Streptococcus mutans* biofilms. The CFUs counting test and CLSM test showed that ALN-GQDs-Ag maintained its antibacterial effect after 24 h of *Streptococcus mutans* biofilm challenge. Meanwhile, the antibacterial effect of silver nitrate was minimised because the results of Group $AgNO_3$ were not significantly different from those of Group Water.

The demineralisation-remineralisation process was employed to investigate cariology by simulating the oral environment in vitro. In this study, the remineralising effects of ALN-GQDs-Ag on artificial caries were investigated. Instead of a pure chemical model, the dynamics of mineral loss and gain in carious formation were mimicked by the periodic alternation of pH produced by biofilm metabolism and artificial saliva. *Streptococcus mutans* biofilms were cultured to create carious lesions before remineralisation with artificial saliva.[25] In micro-CT images, dentine caries treated with ALN-GQDs-Ag presented a shallower lesion depth and higher lesion density on the surface of blocks than those treated with water. The micro-CT results illustrated that ALN-GQDs-Ag were effective in mineralising artificial dentine caries. This could be related to the superior and prolonged antimicrobial effects of Silver nanoparticles against *Streptococcus*

mutans.[26] The more active antibacterial effect of silver nanoparticles is associated with less acidic products by biofilm metabolism of *Streptococcus mutans* biofilm, which weakens the intensity of the demineralisation effect. In addition, our test showed that ALN-GQDs-Ag reduced lactic acid production in *Streptococcus mutans* biofilms. Lactic acid constitutes 70% of the organic acids generated in oral biofilms, and is recognised as a crucial factor in the demineralisation of teeth. Thus, the dentine blocks treated with ALN-GQDs-Ag exhibited enhanced acid resistance and reduced demineralisation. Furthermore, graphene materials can foster hydroxyapatite, which is an important component of the mineralisation process.[27] Graphene materials have been demonstrated as bio-ceramic support materials that enhance hydroxyapatite deposition. They can promote mineralisation with accelerated hydroxyapatite growth by forming a coating of homogenous and compacted hydroxyapatite-graphene. This coating consists of flake-shaped hydroxyapatite crystals with markedly elevated calcium phosphate ratios.

When dentine collagen is exposed after mineral loss, activated host-derived collagenases, such as matrix metalloproteinase (MMP) and cysteine cathepsin, are activated in an acidic environment and can destroy the terminal peptide region of collagen molecules.[28] With the degradation of collagen, more minerals are dissolved because of the disappearance of the scaffold for mineral deposition.[29] In the FTIR spectra (Figure 10), the phosphate band represents the mineral, the amide I band represents collagen, and the ratio of amide I to HPO_4^{2-} represents the degree of dentine degradation.[30] The results of this study indicated that collagen degradation was lower in the dentine surface treated with ALN-GQDs-Ag than in those treated with water. Silver can interact with the reactive side chain of bacterial collagenase to inactivate its catalytic functions.[31] The process of collagen degradation was slowed down through the suppression of bacterial collagenase by silver. It has been revealed that the large radius and low oxidation state of silver have a strong affinity to protein, which may contribute to the inhibition of bacterial collagenase.[32] Besides, it has been proved that silver nanoparticles efficiently decreased the mRNA and protein expression of MMP-2 and MMP-9 in diabetic mice.[33] In the XRD patterns, silver chloride (AgCl) was detected on the dentine surface of the ALN-GQDs-Ag group. The solubilities of silver phosphate and silver oxide are higher than that of AgCl, which enables them to react with chlorides to yield AgCl.[34] Insoluble AgCl on the lesion surface can decrease the loss of calcium and phosphate as a protective layer. Silver nanoparticles were observed in the ALN-GQDs-Ag group, which could continuously release silver on the dentine surface.

The discolouration effect of ALN-GQDs-Ag to dentine is measured using Commission International del'Eclairage L* a* b* colour system (CIELAB). The CIELAB colour system provides a standardised way to describe colours, and was used by researchers to evaluate colour change due to application of silver compounds including silver diamine fluoride.[16] The ΔE*ab values were calculated using L, a, and b values to quantify the difference (colour change or distance between the two colour). The colour change is perceptible by human eye when ΔE is larger than 1.[35] In this study, ΔE values of both ALN-GQDs-Ag group and water group are more than 1, but no significant difference between two groups. Thus, the discolouration of dentine can result from the carious lesion after biofilm challenge. This study was a laboratory-based study. In the future, animal studies followed by human clinical trials will be considered to establish the safety and effectiveness of ALN-GQDs-Ag for caries prevention.

Conclusion

Novel tooth-binding and non-discolouring ALN-GQDs-Ag were developed with antibacterial and mineralising properties for caries prevention. ALN-GQDs-Ag has low toxicity towards oral cells and a high affinity to hydroxyapatite, which is the main component of teeth. They have promising antibacterial properties against *Streptococcus mutans* biofilms and mineralising properties towards dentine. ALN-GQDs-Ag could potentially be used as an anti-caries agent.

Acknowledgments

This study was supported by the Health and Medical Research Fund (HMRF 19180782 and 22210782) of the Food and Health Bureau of the Hong Kong Government.

Author Contributions

All authors made a significant contribution to the work reported, whether that is in the conception, study design, execution, acquisition of data, analysis and interpretation, or in all these areas; took part in drafting, revising or critically reviewing the article; gave final approval of the version to be published; have agreed on the journal to which the article has been submitted; and agree to be accountable for all aspects of the work.

Disclosure

The authors declare that they have no known competing financial interests or personal relationships that could influence the work reported in this study.

References

1. Peres MA, Macpherson LM, Weyant RJ, et al. Oral diseases: a global public health challenge. *Lancet*. 2019;394(10194):249–260. doi:10.1016/S0140-6736(19)31146-8
2. Dimopoulou M, Antoniadou M, Amargianitakis M, Gortzi O, Androutsos O, Varzakas T. Nutritional factors associated with dental caries across the lifespan: a review. *Appl Sci*. 2023;13(24):13254.
3. Nyvad B, Takahashi N. Integrated hypothesis of dental caries and periodontal diseases. *J Oral Microbiol*. 2020;12(1):1710953. doi:10.1080/20002297.2019.1710953
4. Nizami MZI, Xu VW, Yin IX, Yu OY, Chu C-H. Metal and metal oxide nanoparticles in caries prevention: a review. *Nanomaterials*. 2021;11(12):3446.
5. Nizami MZI, Xu VW, Yin IX, Lung CYK, Niu JY, Chu CH. Ceramic nanomaterials in caries prevention: a narrative review. *Nanomaterials*. 2022;12(24):4416. doi:10.3390/nano12244416
6. Walsh T, Oliveira-Neto JM, Moore D. Chlorhexidine treatment for the prevention of dental caries in children and adolescents. *Cochrane Database Syst Rev*. 2015;4.
7. Buzalaf MAR, Pessan JP, Honório HM, Ten Cate JM. Mechanisms of action of fluoride for caries control. *Fluoride Oral Environm*. 2011;22:97–114.
8. Mei ML, Lo EC, Chu C. Arresting dentine caries with silver diamine fluoride: what's behind it? *J Dental Res*. 2018;97(7):751–758. doi:10.1177/0022034518774783
9. Yin IX, Zhang J, Zhao IS, Mei ML, Li Q, Chu CH. The antibacterial mechanism of silver nanoparticles and its application in dentistry. *Int J Nanomed*. 2020;Volume 15:2555–2562. doi:10.2147/IJN.S246764
10. Yin IX, Zhao IS, Mei ML, Li Q, Yu OY, Chu CH. Use of silver nanomaterials for caries prevention: a concise review. *Int J Nanomed*. 2020;Volume 15:3181–3191. doi:10.2147/IJN.S253833
11. Xu X, Chen X, Li J. Natural protein bioinspired materials for regeneration of hard tissues. *J Mat Chem B*. 2020;8(11):2199–2215. doi:10.1039/D0TB00139B
12. Nizami MZI, Yin IX, Lung CYK, Niu JY, Mei ML, Chu CH. In vitro studies of graphene for management of dental caries and periodontal disease. *A Concise Rev Pharmaceutics*. 2022;14(10):1997.
13. Rahat R, Umar K, Umar S, et al. Graphene quantum dots: application in biomedical science. *Graphene Quantum Dots*. 2023:101–111
14. Javadian S, Najafi K, Sadrpoor SM, Ektefa F, Dalir N, Nikkhah M. Graphene quantum dots based magnetic nanoparticles as a promising delivery system for controlled doxorubicin release. *J Mol Liq*. 2021;331:115746. doi:10.1016/j.molliq.2021.115746
15. Dong Y, Shao J, Chen C, et al. Blue luminescent graphene quantum dots and graphene oxide prepared by tuning the carbonization degree of citric acid. *Carbon*. 2012;50(12):4738–4743. doi:10.1016/j.carbon.2012.06.002
16. Yin IX, Yu OY, Zhao IS, et al. Developing biocompatible silver nanoparticles using epigallocatechin gallate for dental use. *Arch Oral Biol*. 2019;102:106–112. doi:10.1016/j.archoralbio.2019.03.022
17. Tian P, Tang L, Teng K, Lau S. Graphene quantum dots from chemistry to applications. *Mater Today Chem*. 2018;10:221–258.
18. Roy D, Kanojia S, Mukhopadhyay K, Eswara Prasad N. Analysis of carbon-based nanomaterials using Raman spectroscopy: principles and case studies. *Bull Mater Sci*. 2021;44(1):31. doi:10.1007/s12034-020-02327-9
19. Beasley MM, Bartelink EJ, Taylor L, Miller RM. Comparison of transmission FTIR, ATR, and DRIFT spectra: implications for assessment of bone bioapatite diagenesis. *J Archaeol Sci*. 2014;46:16–22. doi:10.1016/j.jas.2014.03.008
20. Chen S, Hai X, Chen X-W, Wang J-H. In situ growth of silver nanoparticles on graphene quantum dots for ultrasensitive colorimetric detection of H2O2 and glucose. *Anal Chem*. 2014;86(13):6689–6694. doi:10.1021/ac501497d
21. Mohagheghpour E, Farzin L, Sadjadi S. Alendronate-functionalized graphene quantum dots as an effective fluorescent sensing platform for arsenic Ion detection. *Biol Trace Elem Res*. 2023;1–11.
22. Mikhailova EO. Silver nanoparticles: mechanism of action and probable bio-application. *J Functional Biomater*. 2020;11(4):84. doi:10.3390/jfb11040084
23. Mukherji S, Bharti S, Shukla G, Mukherji S. Synthesis and characterization of size-and shape-controlled silver nanoparticles. *Phys Sci Rev*. 2019;4(1):20170082. doi:10.1515/psr-2017-0082
24. Chen S, Guo R, Xie C, Liang Q, Xiao X. Biomimetic mineralization of nanocrystalline hydroxyapatites on aminated modified polylactic acid microspheres to develop a novel drug delivery system for alendronate. *Mater Sci Eng C*. 2020;110:110655. doi:10.1016/j.msec.2020.110655
25. Yu OY, Zhao IS, Mei ML, Lo EC-M, Chu C-H. A review of the common models used in mechanistic studies on demineralization-remineralization for cariology research. *Dentistry J*. 2017;5(2):20. doi:10.3390/dj5020020
26. Collado-González M, García-Bernal D, Oñate-Sánchez RE, et al. Cytotoxicity and bioactivity of various pulpotomy materials on stem cells from human exfoliated primary teeth. *Int Endodontic J*. 2017;50(S2):e19–e30. doi:10.1111/iej.12751

27. Wei G, Gong C, Hu K, Wang Y, Zhang Y. Biomimetic hydroxyapatite on graphene supports for biomedical applications: a review. *Nanomaterials*. 2019;9(10):1435. doi:10.3390/nano9101435
28. Tjäderhane L, Buzalaf MAR, Carrilho M, Chaussain C. Matrix metalloproteinases and other matrix proteinases in relation to cariology: the era of 'Dentin Degradomics'. *Caries Res*. 2015;49(3):193–208. doi:10.1159/000363582
29. Tay FR, Pashley DH. Guided tissue remineralisation of partially demineralised human dentine. *Biomaterials*. 2008;29(8):1127–1137. doi:10.1016/j.biomaterials.2007.11.001
30. Yip HK, Guo J, Wong WHS. Protection offered by root-surface restorative materials against biofilm challenge. *J Dental Res*. 2007;86(5):431–435. doi:10.1177/154405910708600508
31. Zhao IS, Gao SS, Hiraishi N, et al. Mechanisms of silver diamine fluoride on arresting caries: a literature review. *Int Dental J*. 2018;68(2):67–76. doi:10.1111/idj.12320
32. Baici A, Camus A, Marsich N. Interaction of the human leukocyte proteinases elastase and cathepsin G with gold, silver and copper compounds. *Biochem Pharmacol*. 1984;33(12):1859–1865. doi:10.1016/0006-2952(84)90540-9
33. Krishnan N, Velramar B, Ramatchandirin B, et al. Effect of biogenic silver nanocubes on matrix metalloproteinases 2 and 9 expressions in hyperglycemic skin injury and its impact in early wound healing in streptozotocin-induced diabetic mice. *Mater Sci Eng C*. 2018;91:146–152. doi:10.1016/j.msec.2018.05.020
34. Yu OY, Zhao IS, Mei ML, Lo ECM, Chu CH. Caries-arresting effects of silver diamine fluoride and sodium fluoride on dentine caries lesions. *J Dentistry*. 2018;78:65–71. doi:10.1016/j.jdent.2018.08.007
35. Minaker SA, Mason RH, Chow DR. Optimizing color performance of the ngenuity 3-dimensional visualization system. *Ophthalmol Sci*. 2021;1(3):100054. doi:10.1016/j.xops.2021.100054